Progress in MOVPE of HgCdTe for Advanced Infrared Detectors

P. MITRA,[1] F.C. CASE,[1] and M.B. REINE[2]

1.—Lockheed Martin Vought Systems, Dallas, TX 75265. 2.—Lockheed Martin IR Imaging Systems, Lexington, MA 02173

This paper reviews the significant progress made over the past five years in the development of metalorganic vapor phase epitaxy (MOVPE) for the *in situ* growth of HgCdTe p-n junction devices for infrared detector arrays. The two basic approaches for MOVPE growth of HgCdTe, the interdiffused multilayer process (IMP), and direct alloy growth (DAG) are compared. The paper then focuses on the progress achieved with the IMP approach on lattice-matched CdZnTe substrates. The benefits of the precursors ethyl iodide (EI) and *tris*-dimethylaminoarsenic (DMAAs) for controlled iodine donor doping and arsenic acceptor doping at dopant concentrations relevant for HgCdTe junction devices are summarized along with the electrical and lifetime properties of n-type and p-type HgCdTe films grown with these precursors. The relative merits of the two CdZnTe substrate orientations we have used, the (211)B and the (100) with 4°–8° misorientation are compared, and the reasons why the (211)B is preferred are discussed. The growth and repeatability results, based on secondary ion mass spectrometry analysis, are reported for a series of double-heterojunction p-n-N-P dual-band HgCdTe films for simultaneous detection in the 3–5 μm and 8–10 μm wavelength bands. Finally, the device characteristics of MOVPE-IMP *in situ* grown p-on-n heterojunction detectors operating in the 8–12 μm band are reviewed and compared with state-of-the-art liquid phase epitaxial grown devices.

Keywords: HgCdTe, infrared detectors, interdiffused-multilayer-process

INTRODUCTION

It is becoming increasingly apparent that advanced HgCdTe infrared (IR) detector technology will be based on bandgap-engineered device architectures that will be grown *in situ* by vapor phase epitaxy. Examples of such devices include improved single-color junction structures with various buffer/contact layers, p-on-n heterojunctions with precisely placed p-n transitions, simultaneous dual-band detectors for mid wave (MW)/long wave (LW), MW/MW, and LW/LW, three-color detectors, devices with *in situ* passivation, devices grown on silicon substrates, avalanche photodiodes, and others that are yet to be demonstrated. These device structures require the growth of precisely tailored multiple alloy compositions of HgCdTe as well as controlled p-type and n-type doping with near 100% activation efficiency. Increasingly, such advanced device structures are becoming possible because of the advances being achieved in molecular beam epitaxy (MBE)[1–7] and metalorganic vapor phase epitaxy (MOVPE).[8–14]

There has been significant progress in MOVPE growth of high quality HgCdTe and in controlled doping with high electrical activation efficiency for both donors and acceptors. The mobilities and minority carrier lifetimes now routinely achieved for extrinsically doped n-type and p-type films follow essentially the same trends observed in state-of-the-art liquid phase epitaxy (LPE) grown HgCdTe. These advances have led to *in situ* growth of high quality detectors and detector arrays in various configurations. These include p-on-n heterojunctions in LW and MW spectral bands, n-on-p heterojunctions for MW detectors, p-n-N-P simultaneous dual-band detectors and arrays and non-equilibrium Auger suppressed LW detectors.

Earlier work on the fundamental issues of MOVPE growth and doping has been reviewed by Hicks,[15] Maxey, [16] Mullin and Irvine[17] and Irvine.[18] This paper provides an overview of the recent advances in MOVPE of HgCdTe, with emphasis on those aspects of the

(Received February 1, 1998; accepted February 15, 1998)

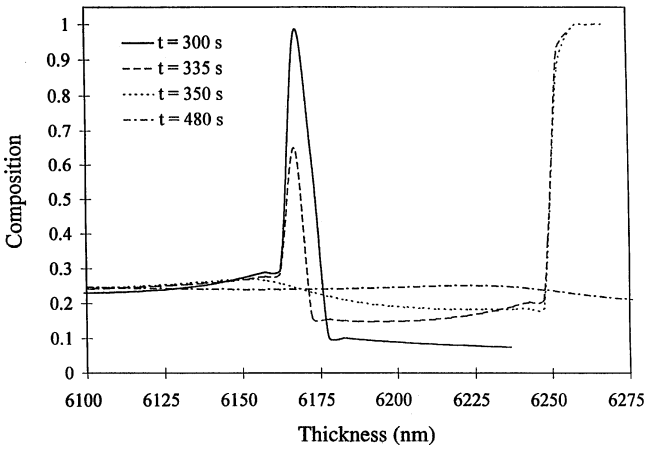

Fig. 1. Composition profiles vs thickness modeled from laser reflectance data for a portion of an MOVPE-IMP growth run for x = 0.23 HgCdTe at different times as indicated (reproduced from Ref. 22).

technology necessary for the growth of p-n junctions including n-type and p-type doping and *in situ* growth of LW and MW p-n junction devices on lattice-matched CdZnTe substrates.

MOVPE GROWTH APPROACH: IMP vs DAG

There are two approaches for MOVPE growth of HgCdTe: one based on direct growth of the ternary alloy - direct alloy growth (DAG),[19] and the second based on interdiffused formation of the ternary following initial deposition of alternating thin layers of HgTe and CdTe with total period thicknesses of ≤150 nm. The latter approach, known as the interdiffused multilayer process (IMP),[20] takes advantage of the rapid interdiffusion rates (D~ 10^{-11}–10^{-13}cm^2/s) of the cations in HgTe and CdTe at the typical growth temperatures in the range of 350–380°C. In IMP, the alloy composition is determined by the relative thicknesses of the binaries which are simply controlled by adjusting the times for their growth.

The time evolution of the cation interdiffusion in IMP MOVPE growth of HgCdTe has been elegantly demonstrated by monitoring the laser reflectance signal[21] and modeling the interdiffusion process.[22] Figure 1 shows a sequence of four calculated compositional profiles[22] for an IMP structure with 93.6 nm of HgTe and 27.6 nm of CdTe. The growth run was carried out at 380°C. The first profile, taken at t = 300 s, into the growth run during the HgTe growth phase, shows that the rapid diffusion of Cd prevents the formation of 100% HgTe. The preceding CdTe layer narrows due to interdiffusion but retains the CdTe composition near the center. The subsequent period at 335 s is at the start of the next CdTe growth, by which time the preceding CdTe layer achieves a maximum Cd mole fraction of 0.60. Because the diffusion of Cd in HgTe is faster than the diffusion of Hg in CdTe, the CdTe phase remains a binary, unlike the HgTe phase. At 350 s, the Cd mole fraction of the preceding CdTe layer reduces to 0.30 and finally at 480 s the "binaries" approach complete homogenization into the ternary alloy. Thus, within 180 s at the growth temperature of 380° C interdiffusion of the IMP cycle is virtually complete to the homogenized alloy. Furthermore, the results of Fig. 1 show that during the HgTe growth phase, the interdiffusion process is so rapid that the surface composition never reaches that of the binary. By contrast, the thinner CdTe layer does achieve the binary composition initially but the Cd rapidly diffuses into the Hg-rich alloy. The interdiffusion process becomes even more rapid as Cd mole fraction of the peak decreases.

In addition to the relative ease of implementation of IMP, a key benefit lies in the ability to control the II/VI ratio during the CdTe cycle of growth. By controlling the II/VI ratio, dopants can be preferentially "pushed" to the intended lattice site. Furthermore, MOVPE-IMP is readily amenable to straightforward *in situ* monitoring of HgCdTe alloy composition and thickness by measuring optical reflectance,[21] as compared to the more complex technique of spectroscopic ellipsometry required for DAG.[23] In a direct comparison of MOVPE growth of HgCdTe on CdZnTe substrates, in the same reactor by DAG and IMP from a statistically significant number of growth runs, Edwall[24] has shown that lower etch pit densities (EPD), by about a factor of two, are obtained in the DAG material than in the IMP material. Good uniformity in alloy composition and film thicknesses have been demonstrated by both techniques.[24,25] However, except for the work of Rao et al.,[26] *in situ* grown p-n junction device results have not been reported by DAG, whereas a significant body of data now exists for a variety of p-n junction devices grown *in situ* by IMP.[8,11–14,27]

MOVPE GROWTH SYSTEM AND PRECURSORS

There are two basic configurations of growth systems used for MOVPE growth of HgCdTe. They are the vertical geometry reactor, used primarily with DAG, and the horizontal reactor that has been used for both DAG and IMP growth. Our system consists of a horizontal geometry quartz reactor, custom built by Metals Research of UK specifically for IMP growth. The precursors are injected through a common fast flow switching manifold using Pd diffused H_2 gas. A heated elemental Hg reservoir adjacent to the graphite susceptor is the source of Hg vapor which is transported to the substrates with H_2. The Hg reservoir is separated from the path of the organometallic precursor flow to ensure that premature reaction of Hg with DMCd does not occur. The reaction of Hg with DMCd has been established to cause the formation of Cd dust, which results in the formation of polycrystalline hillock defects in the HgCdTe films.[28]

The most common precursors currently being used for HgCdTe growth at 350–380°C are dimethylcadmium (DMCd) and diisopropyltelluride (DIPTe), for Cd and Te, respectively. The MOVPE growth temperature is primarily determined by the dissociation chemistry of the Te precursor since DMCd readily dissociates at 250–180°C. In addition to the

dissociation temperature of the Te-precursor, the choice of the appropriate precusor has to be made based on a number of considerations which include growth temperature, reaction chemistry, stability of the precursor under ambient conditions, and the purity levels at which it can be obtained commercially. For example, methyl allyl telluride (MATe), which has a lower decomposition temperature than DIPTe, has proven to be unsuitable for HgCdTe growth due to the formation of dimethyltelluride and dimethylditelluride.[29] The former has a higher dissociation temperature (>390°C) while the latter is a low volatility compound. For growth at reduced temperatures, ditertiarybutyltelluride may be a promising precursor, using which Yasuda et al.[30] have demonstrated direct alloy growth at 275°C.

Elemental mercury, due to its high vapor pressure, is conveniently transported to the reactor and therefore organometallic precursors are not essential. Moreover, the Hg-alkyls have significantly higher dissociation temperatures and are known to be extremely toxic.

DONOR DOPING

The standard n-type dopant used in epitaxial HgCdTe grown by LPE and MBE is indium. In MOVPE however, the In-precursors are found to react with the Te-alkyls and form low-volatility adducts whose long persistence results in memory effects. Furthermore, they usually have high vapor pressures which make them difficult to control for low-level In-doping at ~1×10^{15} cm^{-3} required for LW p-on-n heterojunctions. The readily available trimethyl-indium has proven to be unsuitable for controlled doping for both of these reasons. With triisopropyl-indium (TIPIn), good control of In-doping was demonstrated by separating the DMCd and DIPTe feed lines and introducing it in the DMCd line.[31] Both IMP[31] and DAG[32] approaches have successfully used TIPIn in this manner and achieved In-doping in the range of 10^{14}–10^{18} cm^{-3} with 100% electrical activation and good mobilities. However, the abrupt doping profiles required in multijunction devices were not demonstrated with this precursor.

The group VII element iodine is another dopant that has been successfully used for n-type doping in bulk,[33] MOVPE[12,34–36] and metalorganic molecular beam epitxy (MOMBE)[37] grown HgCdTe. Initial studies of iodine doping in MOVPE[34] were carried out with elemental I_2 which has a vapor pressure of 0.3 Torr at 25°C. Electrically active donor incorporation was observed at low-10^{15} cm^{-3} doping levels with good mobilities.[34] However, I_2 reacts with DMCd and good control with abrupt doping profiles was not demonstrated. Alkyl iodides have since been found to be preferable. In direct alloy growth, iodine doping from isopropyl iodide has been reported[35] to levels as low as 5×10^{15} cm^{-3}, but a memory effect was observed.

We have demonstrated that ethyl iodide (EI) is a highly effective precursor for donor doping without any memory effects.[36] Controlled iodine doping has been achieved in the range of 3×10^{14}–2×10^{18} cm^{-3} with 100% electrical activation following a standard Hg-rich stoichiometric anneal at 235°C. A double-dilution bubbler configuration has been used to obtain controlled low-level doping. Figure 2 shows secondary ion mass spectrometry (SIMS) depth profile data of a HgCdTe layer with three iodine doping levels and two undoped regions. The iodine profiles are very abrupt, which demonstrates the absence of any memory effects as well as the low diffusivity of iodine in HgCdTe. The relative alloy composition in this layer was measured by the ^{125}Te secondary ion yield, and Fig. 2 shows that, even at the relatively high doping level of 2×10^{17} atoms/cm^3, no significant change in the composition is observed. This demonstrates that EI does not undergo any significant reactions with either the Cd or Te precursors. More recently, controlled low-level doping has also been demonstrated with 2-methylpropyliodide(2MePrI), which has about a tenth of the vapor pressure of EI.[12] Doping results with this precursor are similar to those achieved with EI.

Iodine incorporation efficiency in HgCdTe from EI exhibits a strong dependence on the precise orientation of the CdZnTe substrate.[38] Figure 3 shows the concentration of iodine in HgCdTe grown by MOVPE on CdZnTe, measured by SIMS, for a number of misorientations from the (100) plane toward (111)B. During growth, the EI partial pressure was maintained at a constant 1.81×10^{-6} atm. We note that the iodine concentration varies over a wide range from mid-10^{15} cm^{-3} for (100)8°→(111)A to mid-10^{18} cm^{-3} for the (211)B orientation. This is the only case where such a large orientation effect has been reported for dopant incorporation in HgCdTe. The phenomenon however, is well known for several dopants in GaAs and other III-V semiconductors.

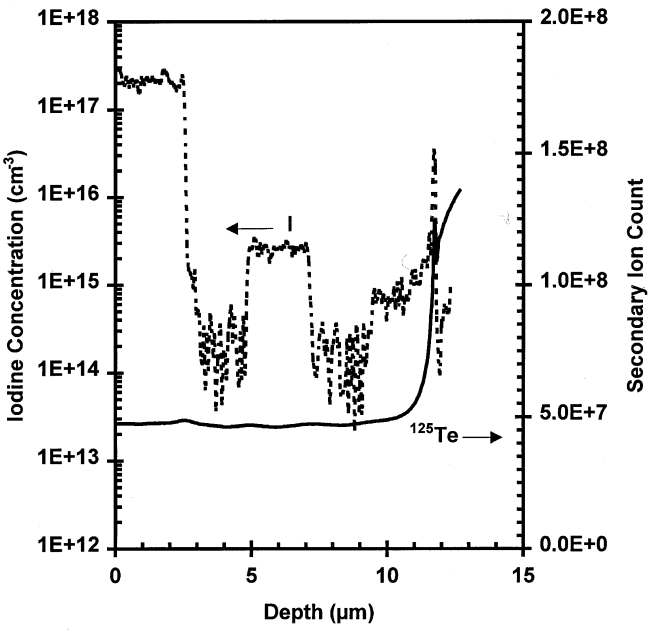

Fig. 2. SIMS depth profile of iodine (dotted line) and the relative alloy composition (^{125}Te profile) in HgCdTe at three different partial pressures.

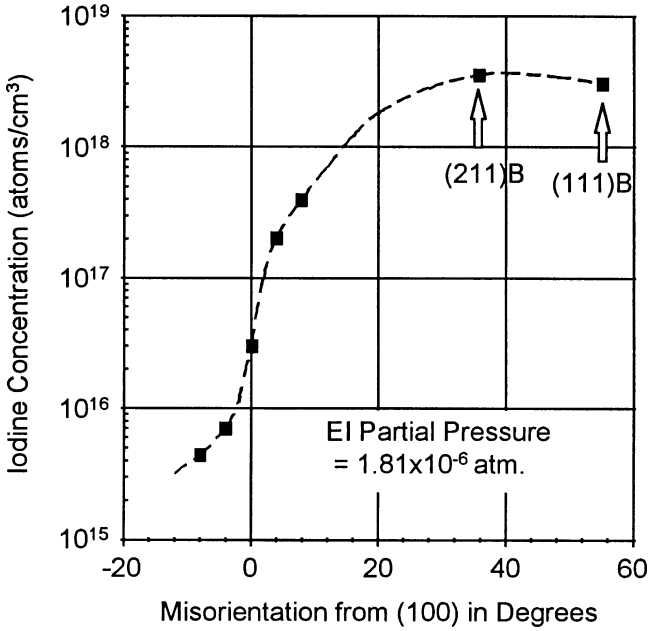

Fig. 3. Iodine incorporation in HgCdTe vs misorientation from the (100) plane toward (111)B measured by SIMS. The partial pressure of EI was constant for all orientations.

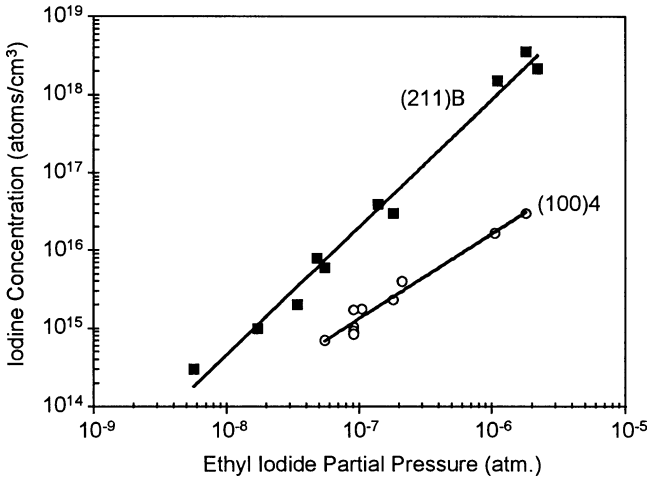

Fig. 4. Iodine incorporation in HgCdTe vs EI partial pressure, measured by SIMS, for the (211)B and (100)4°→(110) orientations.

Figure 4 shows the efficiency of iodine doping as a function of EI partial pressure for two CdZnTe substrate orientations: (100)4°→(110) and (211)B. The growth conditions for both orientations were identical. Iodine concentrations were measured by SIMS. The difference in doping efficiency for the two orientations is clearly evident, with as much as a factor of 100 higher incorporation rate in the (211)B orientation. The high efficiency of iodine incorporation on the technologically significant (211)B orientation makes it more challenging to obtain controlled low-level doping. However, as shown in Fig. 4, doping at levels of low-10^{14} to low-10^{15} cm^{-3} have recently been achieved from EI in a controlled and repeatable manner.

The transport properties of iodine-doped HgCdTe have been characterized extensively in our laboratory. In Fig. 5, the mobilities obtained as a function of composition for iodine-doped and undoped HgCdTe on both (100)4–8°→(111)B and (211)B are shown. Also included is the trend line for state-of-the art LPE grown material.[39] We note that improved mobilities are obtained by iodine doping in MOVPE films, and they are comparable to the liquid phase epitaxy (LPE) data.

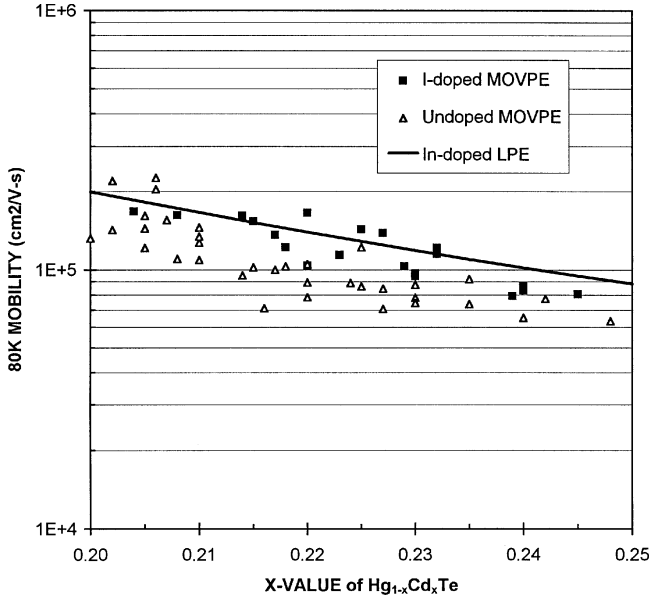

Fig. 5. 80K mobilities of iodine doped and undoped HgCdTe for (100)4-8°→(111)B and (211)B oriented films are compared to In-doped LPE material.

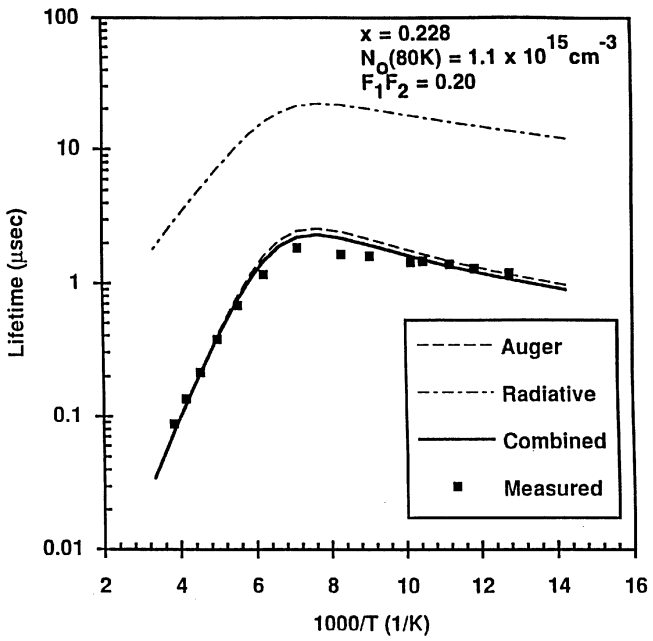

Fig. 6. Temperature dependence of lifetimes measured for an LW iodine doped HgCdTe film grown on (100)4°→(110) CdZnTe and comparison to the theoretical model.

Temperature-dependent lifetime measurements have been carried out using the transient millimeter wave reflectance technique[40] and data for iodine-doped LW and MW HgCdTe are shown in Fig. 6 and

Fig. 7, respectively. The data shown in Fig. 6 and Fig. 7 are for films grown on (100)4°→(110) and (211)B orientations, respectively. Both sets of data agree well with a theoretical model that includes Auger-1 and radiative recombination mechanisms.

ACCEPTOR DOPING

For acceptor doping the most widely used dopant in HgCdTe is arsenic. In MOVPE there have been extensive studies of arsenic doping with a variety of precursors. Early studies in both DAG and IMP used arsine.[16] As less toxic liquid precursors such as tertiarybutylarsine ($TBAsH_2$),[41] and phenylarsine ($PhAsH_2$)[16] became commercially available, they became the preferred alternatives. P-type doping was achieved with both $TBAsH_2$ and $PhAsH_2$ over the range of 3×10^{15}–5×10^{17} cm^{-3} in IMP growth, where the As-precursors are injected in the CdTe growth cycle under Cd-rich conditions. With these precursors a number of *in situ* grown detector configurations have been demonstrated. A key problem with these precursors, however, was that the lifetimes were always significantly lower than those obtained in As-doped HgCdTe grown by Hg-rich LPE. An important clue to this problem is found in the work of Clerjaud et al.[42] who showed that As-doping of CdTe with AsH_3 causes the incorporation of As-H pairs in addition to As. Since As incorporation from $TBAsH_2$ and $PhAsH_2$, both of which are substituted AsH_3, occurs in an analogous manner in MOVPE of HgCdTe, it is likely that As-H pairs are incorporated with these precursors as well.

Recently, *tris*-dimethylaminoarsenic (DMAAs or $[\{CH_3\}_2\text{-}N]_3\text{-}As$) has been found to produce more classical p-type doping.[11,27,43] Unlike $TBAsH_2$ and $PhAsH_2$, DMAAs has no As-H bonds and it is therefore expected that As-H complexes will not be incorporated in the As-doped films. Although As-H complexes are expected to be electrically neutral, they are likely to be recombination centers in HgCdTe and are probably an important factor in the lower lifetimes observed in As-doped films grown with the $TBAsH_2$ and $PhAsH_2$ precursors. DMAAs is also a more convenient precursor for As-doping since its vapor pressure (0.96 Torr at 15°C) is two orders of magnitude lower than that of $TBAsH_2$ at the same temperature. Furthermore, the dissociation of DMAAs is ~50% as compared to ~10% in $TBAsH_2$ at the MOVPE growth temperature of 360°C. The more efficient dissociation at a lower temperature at least in part results in higher incorporation efficiency than with $TBAsH_2$ and $PhAsH_2$.

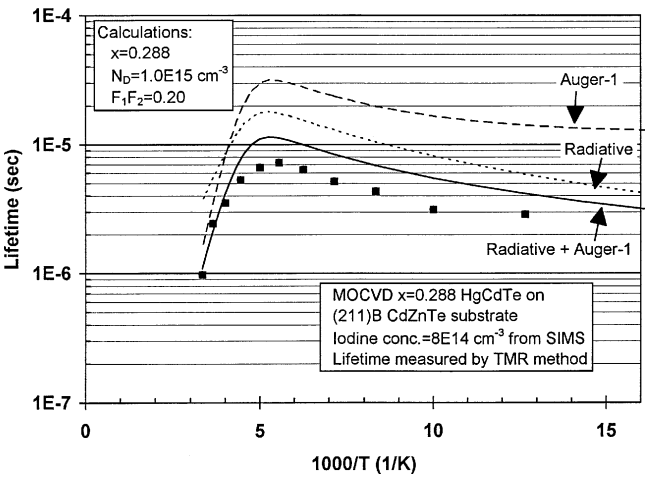

Fig. 7. Temperature dependence of lifetimes measured for an MW iodine doped HgCdTe film grown on (211)B CdZnTe and comparison to the theoretical model.

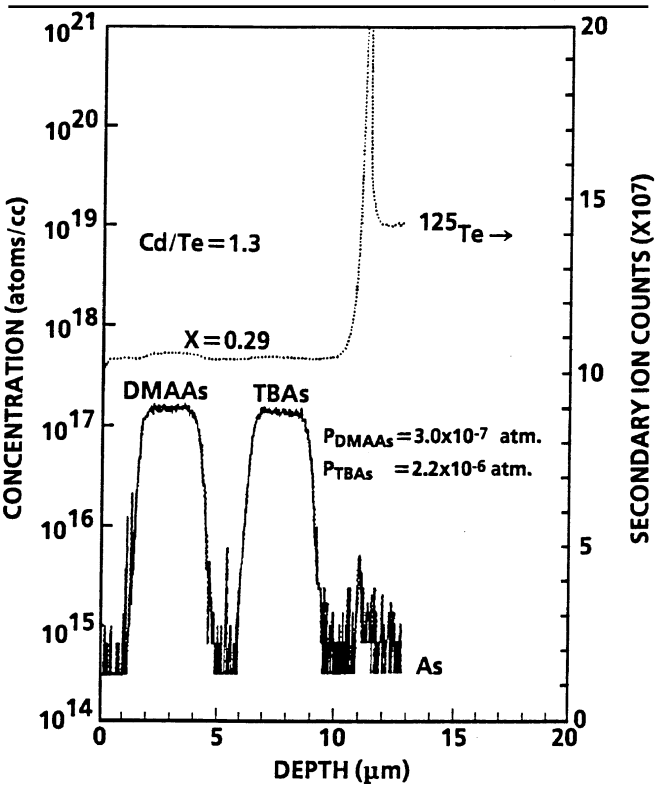

Fig. 8. SIMS depth profiles of As concentration and the relative alloy composition in HgCdTe for doping with $TBAsH_2$ and DMAAs at the indicated partial pressures. Except for switching the As-precursors on and off no other changes were made during the run.

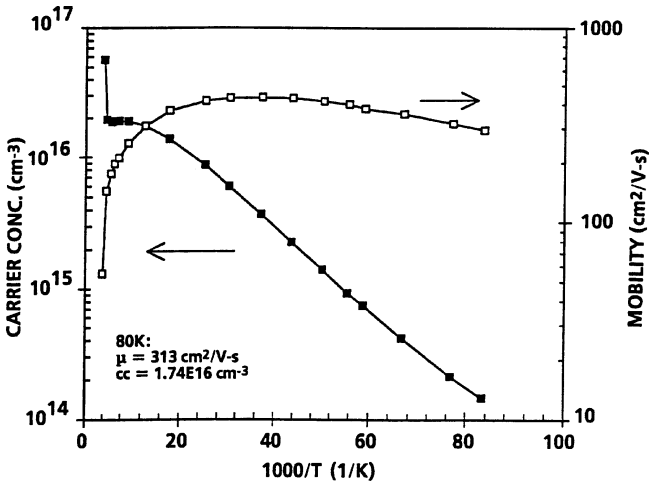

Fig. 9. Temperature dependence of Hall carrier concentration and mobility for As-doped $Hg_{0.70}Cd_{0.30}Te$ with DMAAs. The measurements were performed at 50 kGauss. The film thickness is 9.8 μm.

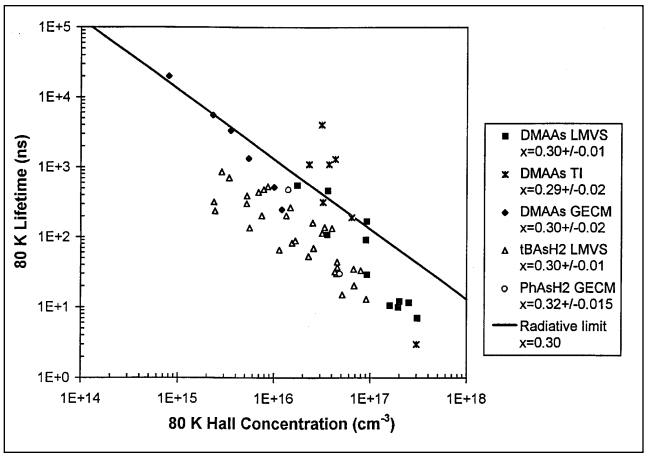

Fig. 10. Summay of 80K lifetimes in As-doped HgCdTe from DMAAs, $TBAsH_2$, and $PhAsH_2$ measured by three different groups. The solid line represents the traditional radiative limit for $Hg_{0.70}Cd_{0.30}Te$ calculated without including reabsorption effects.

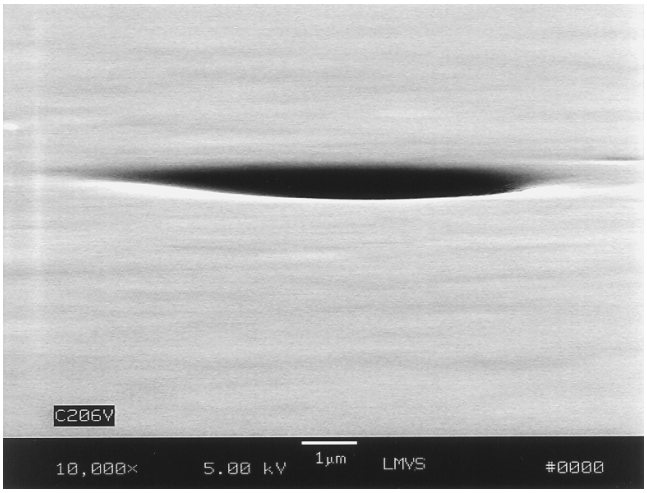

Fig. 11. Scanning electron micrograph of a void defect on HgCdTe grown by MOVPE on (211)B oriented CdZnTe.

Figure 8 shows SIMS depth profile data of a HgCdTe film with two As-doped regions from DMAAs and $TBAsH_2$. The $TBAsH_2$ and DMAAs partial pressures were adjusted to 2.2×10^{-6} and 3.0×10^{-7} atm., respectively, which produced equivalent As concentrations of 1.2×10^{17} cm^{-3}. Thus, to achieve equivalent doping levels, a factor of about 7.3 greater partial pressure of $TBAsH_2$ is required as compared to DMAAs. Figure 8 also shows that relative change in composition is small at these doping levels; the change is estimated to be $\Delta x<0.002$ under the conditions used. At higher doping levels, however, a more significant change in alloy composition has been observed with both precursors.

As-doped HgCdTe from DMAAs following a Hg-rich stoichiometric anneal has not always been found to be fully activated under our growth conditions. Following a Hg-rich anneal at 400°C, however, 100% activation was achieved. This activation anneal temperature is not optimized and lower activation temperature have been demonstrated to suffice.[14,43]

Classical Hall characteristics have been obtained in p-type films doped with DMAAs.[11] An example of the temperature dependence of the mobility and carrier concentration in an x = 0.30 HgCdTe film is shown in Fig. 9. These data along with a number of other measurements at different doping levels have been used to determine the acceptor ionization energies in the As-doped HgCdTe. Model calculations to fit the temperature dependence of the carrier freezeout indicate two shallow acceptor levels are involved with ionization energies of 11.9 and 3.2 meV.[11] These energies are comparable to those reported for As-doped bulk and LPE grown HgCdTe.

Minority carrier lifetime measurements have been reported recently in As-doped HgCdTe grown with $TBAsH_2$ and $PhAsH_2$ and DMAAs precursors by three groups.[14,27,43] The data taken at 80K and plotted as a function of the Hall concentration measured at the same temperature is summarized in Fig. 10. The As-doped MWIR HgCdTe films were grown on both CdZnTe[27,43] and GaAs substrates.[14] It is clear that the lifetimes of the films doped with DMAAs show significantly higher values than those measured in films doped with $TBAsH_2$ and $PhAsH_2$. The 80K lifetimes in the films doped with DMAAs with Hall concentration $\leq 1 \times 10^{17}$ cm^{-3} are close to the traditional radiative limit calculated excluding reabsorption effects and are consistent with lifetimes reported in As-doped Hg-rich LPE grown HgCdTe. The lifetime data reported in Refs. 14 and 27 were on samples without passivation while the samples in Ref. 43 were passivated with anodic oxide. These data provide confidence that As-doping in MOVPE of HgCdTe with DMAAs produces state-of-the-art p-type doping.

SUBSTRATES AND ORIENTATION

A considerable amount of early MOVPE growth of HgCdTe used GaAs substrates despite the ~14% lattice mismatch, due to their consistent and high crystal quality and their availability in larger areas and lower cost. The more technologically significant substrates are lattice-matched CdZnTe for low dislocation HgCdTe and Si because it is inexpensive, available in large areas and thermally matched to the Si readout integrated circuit used in focal plane arrays. Si has ~19% lattice mismatch with HgCdTe and gives rise to higher dislocation densities of $\geq 5 \times 10^6$ cm^{-2}. Nevertheless, since the early work in this area with CdTe/ZnTe/GaAs buffer layers,[44,45] there has been impressive progress on MOVPE growth of CdTe on Si and subsequent growth of HgCdTe.[46,47]

Despite the progress in growth on Si substrates, lattice-matched bulk CdZnTe is the preferred substrate for the growth of the lowest dislocation HgCdTe films which are required for high performance HgCdTe junction devices. At Lockheed Martin, our effort has focused on CdZnTe substrates with a nominal Zn content of 4%. CdZnTe substrates are not without problems, however. Although vast improvements have been made in the crystal quality and purity of commercially available bulk CdZnTe in recent years, fast diffusing impurities such as Cu are sometimes still

found to cause electrical compensation effects in the MOVPE HgCdTe films.[48] Careful selection of high purity CdZnTe substrates is therefore necessary for device quality films.

The crystallographic orientation of the substrate plays a major role in determining the surface morphology of all vapor phase growth techniques for HgCdTe. The most widely commercially available CdZnTe substrates in large areas (such as 4×6 cm^2) have the (111)B orientation. This orientation, however, is not considered practical for MOVPE due to twinning in the HgCdTe layers. The orientation used most often for MOVPE is (100) with a few degrees misoriented toward either (110) or (111)B planes. The (100) HgCdTe films, including those grown on substrates with misorientations ranging from 2°–10° are in general faceted with pyramidal hillock macrodefects.

The precise shape and density of the hillocks depend on the degree of misorientation. A study of homoepitaxy of CdTe by MOVPE on a lenticular substrate has found that, for 4–5°misorientations toward (111)B, hillock-free growth is obtained.[49] However, on HgCdTe grown on CdZnTe substrates with the same misorientation, hillock-free surfaces are not obtained. The hillock density is typically in the range of 50–500 cm^{-2} with sizes ranging from 30–100 μm, depending on the film thickness and the misorientation. Such hillock macrodefects cause outages of elements in detector arrays and thus reduce their operabilty. Certain surface treatments to the (100)2°–4°→(110) GaAs substrates have been recently reported to reduce the hillock density in the growth of HgCdTe/CdTe/GaAs to ≤10 cm^{-2}.[50,51] Various explanations have been proposed for the causes for the formation of these hillock macrodefects in (100) MOVPE HgCdTe.[15,52,53]

When HgCdTe is grown by metalorganic vapor phase epitaxy on the (211)B orientation, no pyramidal hillocks or twinning are observed.[54,55] The (211)B orientation is 35.4° off(100) toward (111)B and has high step densities. This orientation is more promising for high operability detector arrays because the absence of hillock macrodefects makes the film surface much flatter. X-ray double crystal rocking curve widths, etch pit densities, transport properties and p-n junction quality have been found to be essentially equivalent in both the (100) and (211)B orientations. In addition to the surface morphology, the key differences are in the higher growth rates and the higher iodine incorporation efficiency on the (211)B HgCdTe.[38]

We have also found that in MOVPE grown HgCdTe on (211)B CdZnTe, void defects are present with densities ranging from 300–10000 cm^{-2}. A scanning electron micrograph of a void defect is shown in Fig. 11. The (211)B orientation is commonly used in MBE growth of HgCdTe and void defects in HgCdTe were first reported in MBE grown films.[56] We have found the void defects in MOVPE grown HgCdTe are 4–8 μm wide in 10–15 μm thick films and they short the photodiodes fabricated in the area where they are present.

We have found void defects in MOVPE growth to be caused by incomplete cleaning of the CdZnTe substrates as well as by defects native to the substrates themselves. The density of these defects is generally higher than the hillock density in the (100) films, but the sizes of the void defects are significantly smaller. Thus, per macrodefect, more detector outages are expected in an array fabricated from (100) HgCdTe than from (211)B HgCdTe. However, if the void defect density is too high, the advantages of the flatter (211)B surface and smaller macrodefect size become irrelevant. It should be noted that we have not observed any differences in the performance characteristics of MOVPE *in situ* grown LWIR photodiodes fabricated from (100) and (211)B oriented films. Etch pit densities have been measured to be the same as well and have been found to be in the range of (5–20) $\times 10^5$ cm^{-2}.

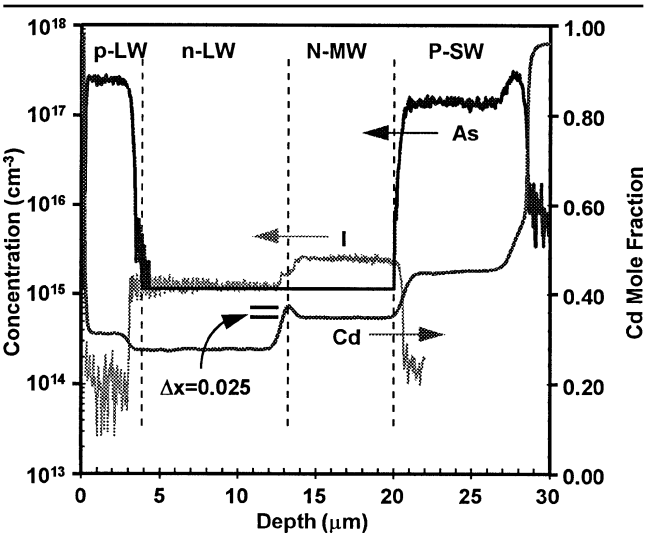

Fig. 12. SIMS depth profile data of the Cd mole fraction, arsenic and iodine doping in a p-n-N-P dual-band HgCdTe film grown with a small composition barrier between the iodine-doped LW and MW absorber layers.

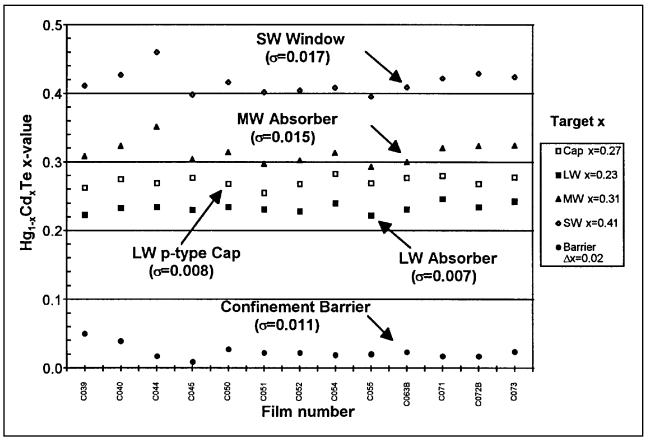

Fig. 13. Repeatability results for x-values for each of the layers in a series of double-heterojunction LW/MW p-n-N-P dual-band films. The target x-values for each layer is shown on the right. The values in parentheses are the standard deviations.

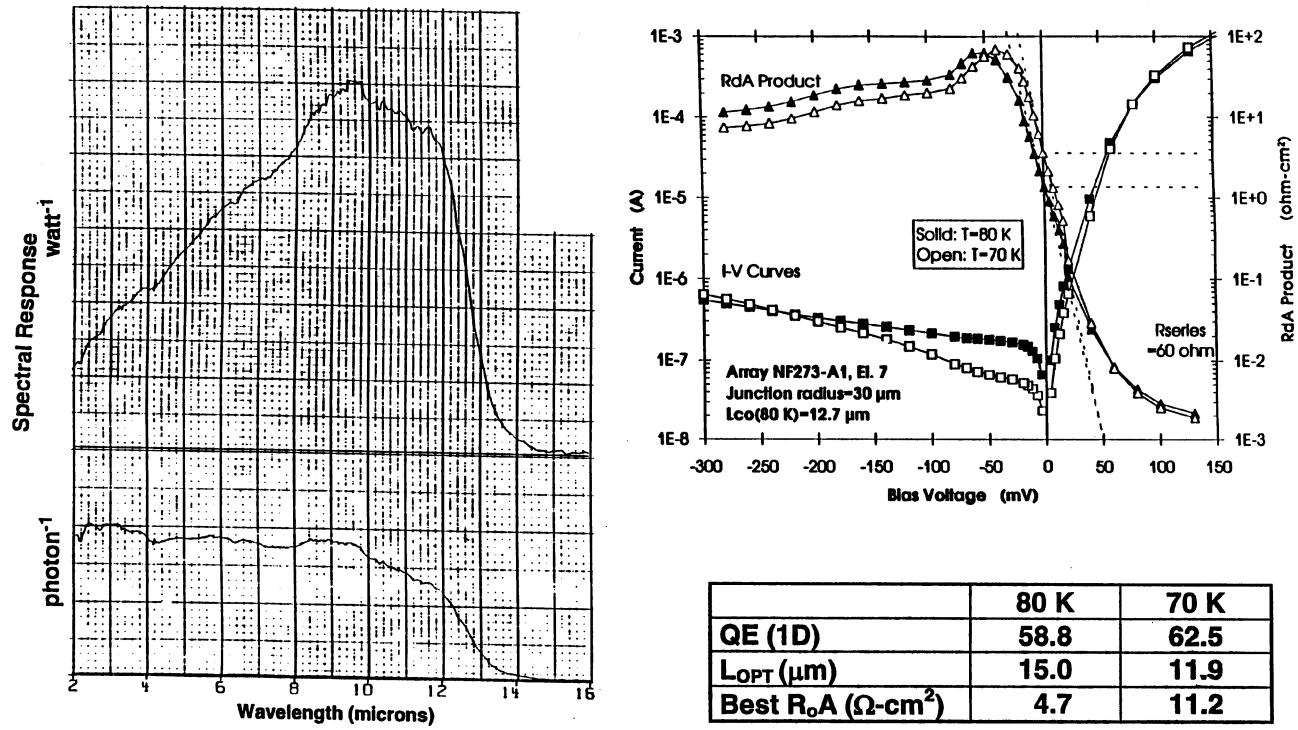

	80 K	70 K
QE (1D)	58.8	62.5
L_{OPT} (μm)	15.0	11.9
Best R_oA (Ω-cm^2)	4.7	11.2

Fig. 14. Spectral response data at 80K (left) I-V curves and R_dA product at 70 and 80K for a photodiode with a junction radius of 30 μm and λ_{co} (80K) = 12.7 μm.

GROWTH CONTROL AND REPEATABILITY

Figure 12 shows SIMS depth profile data taken on a representative p-n-N-P double-heterojunction LW/MW dual-band detector structure grown with a composition barrier between the MW and LW absorber layers. The Cd mole fractions or the x-values were obtained from measurements of the yield of $CsCd^+$ molecular ions resulting from Cs^+ ion bombardment and recombination of the sputtered neutral Cd atoms.[57] The x-value profile clearly shows the well-defined alloy composition regions in the multilayer film structure. The interdiffused widths between layers of different x-values are ≤1.5 μm and are well within acceptable limits for these devices. The small composition barrier between the MW and LW absorber layers is also well-defined, and demonstrates the degree of composition control that is achieved in MOVPE of HgCdTe.

The dopant concentrations in this film were also measured with Cs^+ ion bombardment and quantitated against calibrated standards. The depth profile data for iodine show sharp onset and falloff due to its low diffusion rate in HgCdTe at the growth temperature. The iodine level is at 2×10^{15} cm^{-3} in the MW absorber layer and at 1×10^{15} cm^{-3} in the LW absorber layer, in agreement with the respective target values of $(2–4) \times 10^{15}$ cm^{-3} and $(1–2) \times 10^{15}$ cm^{-3}. The intentionally graded reduction in iodine doping through the barrier layer is also clearly evident. The As-doping levels in the SW p-type layer and the LW p-type cap layer are also well within the targeted values of $(1–2) \times 10^{17}$ cm^{-3} and $(2–4) \times 10^{17}$ cm^{-3}, respectively.

Good run-to-run repeatability in the growth of double-heterojunction dual-band films by MOVPE was demonstrated for a series of 13 films grown with the same parameters. Figure 13 shows the x-value repeatability data for each of the four layers and the confinement barrier. The target values are included along with the standard deviation in x-values for each layer. The x-value of the LW n-type layer was determined by Fourier transform IR transmission measurements and was used to calibrate each of the SIMS x-profiles. The values for each of the layers are close to the target values. The data demonstrate good run-to-run repeatability for this complex multilayer device structure.

DEVICE RESULTS

In this section, we describe the results of LWIR photodiode detectors grown *in situ* in the p-on-n heterojunction configuration. The n-type absorber layers in these films were grown 8–12 μm thick and doped with iodine at $(1–2) \times 10^{15}$ cm^{-3} followed by a p-type cap ~2 μm thick and doped with arsenic at $(2–4) \times 10^{17}$ cm^{-3}. Figure 14 shows the detector characteristics of such a film with a cutoff wavelength of 12.7 μm at 80K. The film was processed into a backside-illuminated variable-area circular mesa photodiode array with ZnS passivation, with no anti-reflection coating. The array was bump interconnected to a circuit board and tested at 70 and 80K. Figure 14

shows the relative spectral responses per photon and per watt, the I-V curves and the dynamic resistance-area product as a function of bias voltage at 80 and 70K. Also shown is a table with the one-dimensional quantum efficiency (QE(1D)) data, the optical collection length L_{opt}, and R_0A, all at 80 and 70K.

Similar MOVPE grown p-on-n LWIR films have been fabricated into mesa-etched backside-illuminated 64×64 arrays with 60×60 μm^2 unit cells. These arrays were passivated with our standard CdTe passivation. The average R_0A and dark current measured at –20 mV for the center 10×10 elements in these arrays are plotted vs the average cutoff wavelength of the photodiodes in Fig. 15, all for a temperature of 77K. Also plotted for comparison are data for arrays fabricated from LPE grown double layer heterojunction films that were processed and tested under the same conditions. Figure 15 includes calculated R_0A and dark current based on the standard model of n-side diffusion current, electron concentration of 1×10^{15} cm^{-3} and lifetimes that follow the Auger-1 mechanism. The data presented in Fig. 14 and Fig. 15 indicate that MOVPE *in situ* grown p-n junctions have progressed to the stage that the LWIR R_0A and dark current results are essentially equivalent to state-of-the-art LPE grown HgCdTe.

SUMMARY AND CONCLUSIONS

This review has shown that MOVPE-IMP has progressed over the past five years to the point that sophisticated bandgap-engineered multilayer HgCdTe device structures can be grown *in situ* on a repeatable and dependable basis.

The MOVPE-IMP approach affords simpler and more direct control of HgCdTe alloy composition than does the DAG approach. It has the additional benefit of allowing adjustment of the II/VI ratio in the CdTe cycle during growth which is critical for efficient dopant incorporation and activation. It also permits straightforward real-time monitoring of alloy composition and thickness based on laser reflectance interferometry.

New dopant precursors have been established: ethyl iodide for iodine donor doping and DMAAs for arsenic acceptor doping. These precursors allow well-controlled *in situ* donor and acceptor doping, at concentrations required for high performance HgCdTe junction photodiodes, with sharp and well-defined depth profiles, and with 100% activation. HgCdTe n-type and p-type films doped from these precursors have electrical and lifetime properties which are equivalent to those of state-of-the-art LPE HgCdTe.

The (211)B CdZnTe substrate orientation is preferred over the (100) CdZnTe orientation because the (211)B film surfaces are free of troublesome pyramidal hillocks. The much higher (100X) iodine incorporation rates in the (211)B HgCdTe can now be readily controlled at concentrations less than 1×10^{15} cm^{-3}. The density of the characteristic void defects present in (211)B films can be reduced to acceptable levels through judicious substrate selection and careful substrate preparation.

Good run-to-run repeatability and control has been demonstrated for a series of 13 identical growth runs of a MW/LW p-n-N-P HgCdTe double-heterojunction dual-band device structure. LW

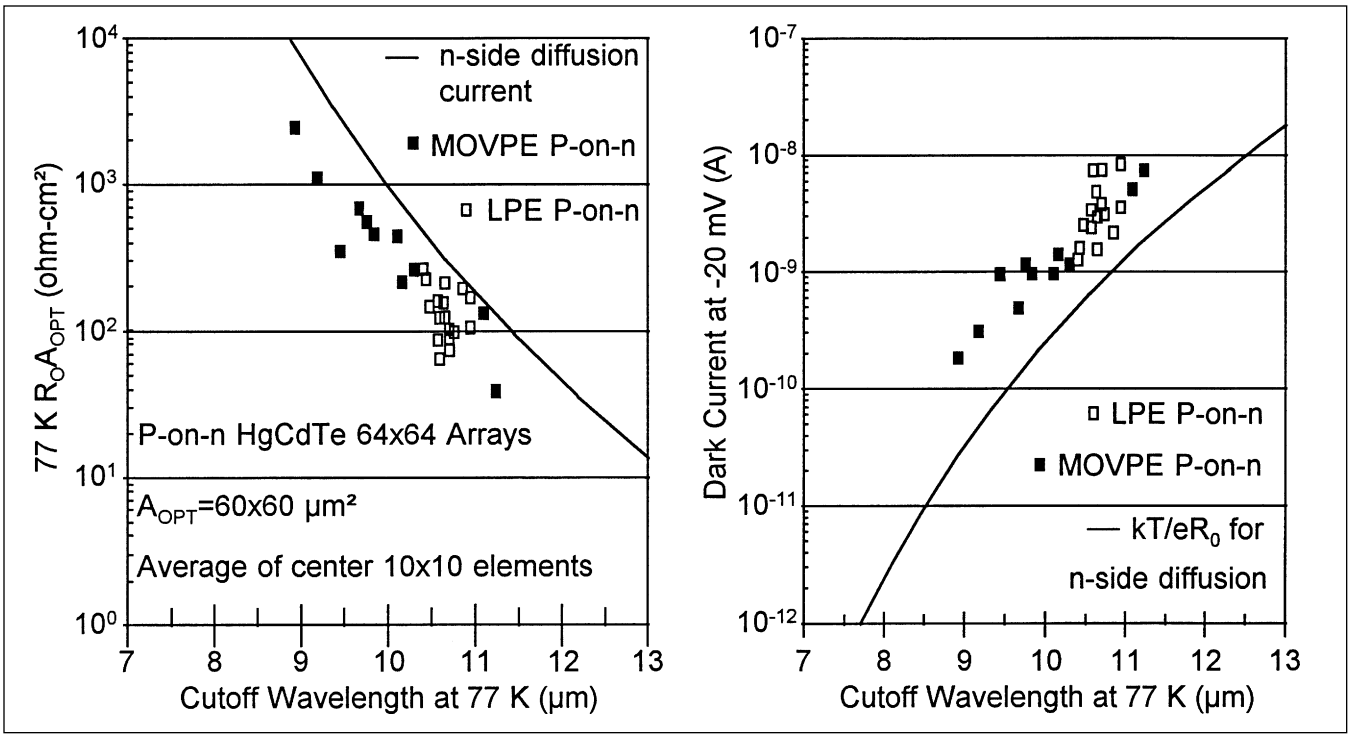

Fig. 15. Comparison of average R_0A and dark current data at 77K, plotted vs cutoff wavelength, for MOVPE and LPE grown HgCdTe photodiode arays. The curves represent calculated values.

P-on-n backside-illuminated CdTe-passivated heterojunction photodiode arrays have shown quantum efficiencies and R_0A products at 77K that are equivalent to those of LPE-grown p-on-n heterojunction arrays fabricated and tested under identical conditions.

The work at Lockheed Martin and elsewhere has revealed that there are no fundamental roadblocks which would prevent the further development of MOVPE into a manufacturable *in situ* growth process. We expect this progress will result from further improvement in the control of growth parameters.

ACKNOWLEDGMENTS

Our MOVPE work has been supported over the years by Naval Research Laboratory (NRL), the Air Force Research Laboratory (AFRL), by Defense Advanced Research Projects Agency (DARPA) and by Lockheed Martin internal research funds. Joseph Omaggio and James Waterman of NRL, Paul LeVan and Ken Brown of AFRL at Kirtland AFB, and Richard Singer of the Institute for Defense Analyses deserve much credit for their active support of this work. We also gratefully acknowledge the contributions made by our colleagues: Austin Brouns and Lewis Claiborne at Lockheed Martin Vought Systems, Peter Norton, Peter O'Dette, Frank Smith, Steve Tobin and Margie Weiler at Lockheed Martin IR Imaging Systems and Tom Casselman at Lockheed Martin Missiles and Space. We also thank Howard Glass of Johnson Matthey for many helpful conversations and inputs on CdZnTe substrates.

REFERENCES

1. J.M. Arias, *Properties of Narrow Gap Cadmium-Based Componds*, EMIS Datareview Series, No. 10, ed. P. Capper, (Inspec, 1994), p. 30.
2. L.A. Almeida, Y.P. Chen, J.P. Faurie, S. Sivananthan, D.J. Smith and S.-C.Y. Tsen, *J. Electron. Mater*. 25, 1402 (1996).
3. T.J. de Lyon, R.D. Rajavel, J.E. Jensen, O.K. Wu, S.M. Johnson, C.A. Cockrum and G.M. Venzor, *J. Electron. Mater*. 25, 1341 (1996).
4. R.D. Rajavel, D.M. Jamba, J.E. Jensen, O.K. Wu, C. Le Beau, J.A. Wilson, E. Patten, K. Kosai, J. Johnson, J. Rosbeck P. Goetz and S.M. Johnson, *J. Electron. Mater.* 26, 476 (1997).
5. O.K. Wu, R.D. Rajavel, T.J. de Lyon, J.E. Jensen, M.D. Jack, K. Kosai, G.R. Chapman, S. Sen, B.A. Baumgratz, B. Walker and B. Johnson, *J. Electron. Mater.* 26, 488 (1997).
6. D.D. Edwall, M. Zandian, A.C. Chen and J.M. Arias, *J. Electron. Mater*. 26, 493 (1997).
7. M.J. Bevan, L.A. Almeida, W.M. Duncan and H.D. Shih, *J. Electron. Mater*. 26, 502 (1997).
8. M.B. Reine, P.W. Norton, R. Starr, M.H. Weiler, M. Kestigian, B.L. Musicant, P. Mitra, T.R. Schimert, F.C. Case, I.B. Bhat, H. Ehsani and V. Rao, *J. Electron. Mater.* 24, 669 (1995).
9. W.S. Wang and I. Bhat, *J. Electron. Mater*. 24, 451 (1995).
10. K. Maruyama, H. Nishino, T. Okamoto, S. Murakami, T. Saito, M. Uchikoshi, M. Nagashima and H. Wada, *J. Electron. Mater*. 25, 1353 (1996).
11. P. Mitra, Y.L. Tyan, F.C. Case, R. Starr and M.B. Reine, *J. Electron. Mater.* 25, 1328 (1996).
12. C.D. Maxey, C.L. Jones, N.E. Metcalfe, R. Catchpole, M.R. Houlton, A.M. White, N.T. Gordon and C.T. Elliott, *J. Electron. Mater.* 25, 1276 (1996).
13. P. Mitra, S.L. Barnes, F.C. Case, M.B. Reine, P. O'Dette, R. Starr, A. Hairston, K. Kuhler, M.H. Weiler and B.L. Musicant, *J. Electron. Mater*. 26, 482 (1997).
14. C.D. Maxey, C.L. Jones, N.E. Metcalfe, R.A. Catchpole, N.T. Gordon, A.M. White and C.T. Elliot, *SPIE Proc.* 3122 (SPIE, 1997), p. 453.
15. R.F. Hicks, *Proc. IEEE* 80 (New York: IEEE, 1992), p. 1625.
16. C.D. Maxey, I.G. Gale, J.B. Clegg and P.A.C. Whiffin, *Semicond. Sci. Technol.* 8, S183 (1993).
17. J.B. Mullin and S.J.C. Irvine, *Prog. Crystal Growth and Charact*. 29, 217 (1994).
18. S.J.C. Irvine, *Narrow-Gap II-VI Compounds for Optoelectronic and Electromagnetic Applications* ed. P. Capper, (London: Chapman & Hall, 1997), p. 30.
19. I.B. Bhat, *J. Cryst. Growth* 117, 1 (1992).
20. J. Tunnicliff, S.J.C. Irvine, O.D. Dosser and J.B. Mullin, *J. Cryst. Growth* 68, 245 (1984).
21. S.J.C. Irvine, J. Bajaj and H.O. Sankur, *J. Cryst. Growth* 124, 654 (1992).
22. S.A. Svoronos, W.W. Woo, S.J.C. Irvine, H.O. Sankur and J. Bajaj, *J. Electron. Mater.* 25, 1561 (1996).
23. S. Dakshina Murthy, I. Bhat, B. Johs, S. Pittal and P. He, *J. Electron. Mater.* 24, 1087 (1995).
24. D.D. Edwall, *J. Electron. Mater.* 22, 847 (1993).
25. S. Murakami, Y. Sakachi, H. Nishino, T. Sato, K. Shinohara and H. Takigawa, *J. Vac. Sci. Technol. B* 10, 1380 (1992).
26. V. Rao, H. Ehsani, I.B. Bhat, M. Kestigian, R. Starr, M.H. Weiler and M.B. Reine, *J. Electron. Mater*. 24, 437 (1995).
27. P. Mitra, T.R. Schimert, F.C. Case, S.L. Barnes, M.B. Reine, R. Starr, M.H. Weiler and M. Kestigian, *J. Electron. Mater.* 24, 1077 (1995).
28. J.E. Hails, I.R. Girling and D.R. Stern, *Mater. Res. Soc. Symp. Proc.* 204 (Pittsburgh, PA: Mater. Res. Soc., 1991), p. 155.
29. J.E. Hails, D.E. Cole-Hamilton and W. Bell, *J. Cryst. Growth* 145, 74 (1994).
30. K. Yasuda, H. Hatano, T. Ferid, K. Kawamoto, T. Maejima and M. Minamide, *J. Electron. Mater.* 24, 1093 (1995).
31. S.J.C. Irvine, J. Bajaj, L.O. Bubulac, W.P. Lin, R.W. Gedridge, Jr. and K.T. Higa, *J. Electron. Mater.* 22, 859 (1993).
32. R. Korenstein, P.H. Hallock, D.L. Lee, E. Sullivan, R.W. Gedridge, Jr. and K.T. Higa, *J. Electron. Mater.* 22, 853 (1993).
33. H.R. Vydyanath and F.A. Kroger, *J. Electron. Mater.* 11, 111 (1982).
34. B.C. Easton, C.D. Maxey, P.A.C. Whiffin, J.A. Roberts, I.G. Gale, F. Grainger and P. Capper, *J. Vac. Sci. Technol. B* 9, 1682 (1991).
35. S. Murakami, T. Okamoto, K. Maruyama and H. Takigawa, *Appl. Phys. Lett.* 63, 899 (1993).
36. P. Mitra, Y.L. Tyan, T.R. Schimert and F.C. Case, *Appl. Phys. Lett*. 65, 195 (1994).
37. R.G. Benz II, A. Conte-Matos, B.K. Wagner and C.J. Summers, *Appl. Phys. Lett.* 65, 2836 (1994).
38. P. Mitra, F.C. Case, M.B. Reine, R. Starr and M.H. Weiler, *J. Cryst. Growth* 170, 542 (1997).
39. S. Tobin, personal communication.
40. A.J. Brouns, T.R. Schimert, P. Mitra, F.C. Case, S.L. Barnes and Y.L. Tyan, *Semicond. Sci. Technol*. 9, 928 (1993).
41. D. Edwall, L.O. Bubulac and E.R. Gertner, *J. Vac. Sci. Technol. B* 10, 1423 (1992).
42. B. Clerjaud, D. Cote, L. Svob, Y. Marfaing and R. Druilhe, *Solid State Comm.* 85, 167 (1993).
43. M.J. Bevan, M.C. Chen and H.D. Shih, *Appl. Phys. Lett.* 67, 3750 (1995).
44. S.M. Johnson, J.A. Vigil, J.B. James, C.A. Cockrum, W.H. Konkel, M.H. Kalisher, R.F. Risser, T. Tung, W.J. Hamilton, W.L. Ahlgren and J. M. Myrosynk, *J. Electronic Mater.* 22, 835 (1993).
45. S.J.C. Irvine, J. Bajaj, R.V. Gil and H. Glass, *J. Electron. Mater.* 24, 457 (1995).
46. K. Shigenaka, K. Matsushita, L. Sugiura, F. Nakata, K. Hirahara, M. Uchikoshi, M. Nagashima and H. Wada, *J. Electron. Mater.* 25, 1347 (1996).
47. T. Okamoto, T. Saito, S. Murakami, H. Nishino, K. Maruyama, Y. Nishijima, H. Wada, M. Nagashima and Y. Nogami, *Appl. Phys. Lett.* 69, 677 (1996).
48. R. Korenstein, R.J. Olson, D. Lee, P.K. Liao and C.A. Castro,

J. Electron. Mater. 24, 511 (1995).
49. D.W. Snyder, S. Mahajan, E.I. Ko and P.J. Sides, *Appl. Phys. Lett.* 58, 848 (1991).
50. J. Geiss, J.E. Hails, A. Graham, G. Blackmore, M.R. Houlton, J. Newey, M.L. Young, M.G. Astles, W. Bell and D.J. Cole-Hamiliton, *J. Electron. Mater.* 24, 1149 (1995).
51. S.-H. Suh, J.-H. Song and S.-W. Moon, *J. Cryst. Growth* 159, 1132 (1996).
52. K. Yong, P.J. Sides and A.J. Gellman, *J. Electron. Mater.* 26, 1261 (1997).
53. J.E. Hails, D.J. Cole-Hamilton and J. Geiss, 1997 U.S. Workshop on the Physics & Chemistry of II-VI Materials, Santa Barbara, CA.
54. G. Cinader, A. Raizman and A. Sher, *J. Vac. Sci. Technol. B* 9, 1634 (1991).
55. M.J. Bevan, N.J. Doyle and T.A. Temofonte, *J. Appl. Phys.* 71, 204 (1992).
56. M. Zandian, J.M. Arias, J. Bajaj, J.G. Pasko, L.O. Bubulac and R.E. DeWames, *J. Electron. Mater*. 24, 1207 (1995).
57. J. Sheng, L. Wang, G.E. Lux and Y. Gao, *J. Electron. Mater*. 26, 588 (1997).